Structural integrity evaluation of cyclic loading glass fibre reinforced polymer composite by acoustic emission and heat transfer

Structural integrity evaluation of cyclic loading GFRP composite by Acoustic Emission and Heat Transfer

Loganathan T G[1], Vinoth Kumar K [2] , Klaudio Bari[3], Hemadri Chadalavala[2], Venkatachalam G[4],

[1]Prof, Department of Mechanical Engineering, RMK College of Engineering and Technology, RSM Nagar, Puduvoyal- 601206, Tamil Nadu, India. Email: dhanushaudi@gmail.com, ORCID: https://orcid.org/0000-0002-8378-1812

[2]Asst. Prof, Department of Mechanical Engineering, RMK College of Engineering and Technology, RSM Nagar, Puduvoyal- 601206, Tamil Nadu, India. Email: skvinothpec@gmail.com, hemadric@rmkcet.ac.in

[3]Professor, School of Engineering, University of Wolverhampton, United Kingdom, Email: k.bari@wlv.ac.uk

[4] Prof, Centre for innovation and product development, School of Mechanical Engineering, Vellore Institute of Technology (VIT), VIT Chennai Campus, Vandalur-Kelambakkam Road, Chennai - 600127. India. Email: g.venkatachalam@vit.ac.in

[5]Asso. Prof, Department of Mechanical Engineering, RMK Engineering College, RSM Nagar, Kavaripettai-601206, Tamil Nadu, India. Email: gmn.mech@rmkec.ac.in

Abstract: GFRP composites are widely employed for static and dynamic loading, which induces structural changes in terms of matrix cracking, debonding, delamination, and fiber failure. In this work, the composite laminate of configuration 0/30/60/0 and 0/90/90/0 of fiber volume fraction V_f = 32% and 25% have been prepared by hand-layup technique and exposed to a cyclic load at 2.6, 4.6, 8.6 Hz. The structural stability of the specimens before and after cyclic load was examined in terms of acoustic emission and heat transfer changes. The peak frequency ranges for the above damage phenomenon of laminates were in the range of 50-100, 110-230, 245-380 kHz variations in AE event count. A matrix dominant behavior is observed with minimum variation in AE activity in lower fiber angle interaction laminate which is missing on increasing fiber interaction angle. Thus, the fiber orientation angle and fiber volume fraction are significant in the retention of structural integrity on cyclic loading. The step heat thermography exhibits minimum ΔT for moderate loading frequency and ΔT drops well below the virgin, insisting in-situ thermography to study the dynamic changes in composites.

Keywords: GFRP, Cyclic Loading, fiber orientation, volume fraction, flexural modulus and Acoustic Emission, Heat Transfer.

1. Introduction

Enhancing the requirements of structural components has driven engineers to evolve newer materials with high specific weight, tailorable properties, high energy absorption, and adaptability to take the complex part profiles. In this scenario, composites have taken their role as the best alternative to conventional metals. There are some unexplored areas in the composite materials, which require further investigation to understand their behavior at varying operating conditions. In the case of fiber-reinforced composites, the general concern is to study their resistance to static as well as dynamic loading.

The damage caused by dynamic loading (fatigue/ cyclic) is very complex in composites because of their anisotropy and mostly causes stress gradients in the structure [1]. This sort of damage is complex combined with anisotropies, non-linear behavior, and distributed throughout the specimen leading to performance degradation. The flowing section describes, the work done on factors affecting the dynamic behavior of composite structures,

the use of techniques like acoustic emission (AE)[2] [3] [4], and thermography in analyzing damages.

The effect of loading [5], [6] and fiber orientation on bending stiffness and strength reduction of composite laminates was attempted by many. In those attempts, the transverse cracks are more predominant in cross-ply contributing to the reduction in stiffness than in an angle ply laminate. The fiber orientation has [7] a significant effect on the degradation of transverse and longitudinal stiffness of the composites. Nevertheless, for high fatigue performance, fiber lay-up should not be orthogonal with respect to the loading axis. Moreover, the damage propagation was minimized by having angle ply laminated surmounting cross-ply [8]. Along with fiber orientation, fiber volume fraction has also contributed to fatigue resistance. The fiber density has a positive effect on the fatigue performance exhibiting a threshold value for V_f = 60% beyond which the failure transforms from tensile to brittle[9], [10].

In a dynamic loading environment along with the load magnitude, the rate of loading is given importance. The effect of load rating on the ILSS of composites was found to have a negative effect on fatigue performance [11]. This is due to the fact that a higher loading rate (high frequency) has minimum time for the matrix to transfer the load to fiber thus contributing to the reduced ILSS and vice versa. As a whole, the visco-elastic nature of the polymer resin combined with load rate positively changes the failure mode from fiber to the matrix [1], [12][13]. On varying strain rates from $0.0016s^{-1}$ to $542s^{-1}$, the tensile strength and modulus of glass/epoxy composites were found to exhibit a rise of 66.3% attributed to the fiber stiffening mechanism of the composite. However, there is a limit on the rise of strain rate and at a very high strain rate, the short loading duration propagates damage faster, leading to lower strain to failure and matrix dominant brittle failure in the fiber-reinforced epoxy composite [1], [14].

The load-induced damage pattern of composite is quite complex which comprises sequential occurrences of matrix cracking/ crazing (MC), fiber-matrix debonding, delamination (D/D), and fiber failure (FF). Other than, the mechanical way of evaluating damages, methods like Acoustic Emission and thermography were implemented for analyzing damages both in-situ and ex-situ conditions [15], [16].

The damage of material under stress normally experiences yielding, cumulative yielding, threshold-cross over, initiation of crack, crack propagation, and failure. Every state of the material is accompanied by a certain degree of relaxation of the stored energy termed as acoustic emission. Acoustic Emission is a weak signal of low amplitude with high frequency. AE is an intelligent, active signal indicating the status/response of a material to a stressed environment. The captured AE signals are examined to describe the behavior of the material along with the induced stresses[17]. It was reported that, the AE data comprises of low frequency – low amplitude, low frequency – high amplitude and high-frequency clusters of AE events, which are correlated with matrix crazing/cracking, debonding and fiber failure respectively[18], [19].

The sensitivity of AE evaluation was demonstrated in assessing the contribution of porosity/voids on the flexural performance of impact-loaded CFRP laminates. The observed AE events reflected the effect of porosity/voids on the delamination resistance of the composite in terms of varying AE energy and counts [20]. Similarly, the compression after the impact of the specimen reveals a frequency range from 100 – 400 kHz for the damages mechanism comprising of matrix cracking, intra and inter-yarn debonding, the breakage of the impact-defected-fibers, and the breakage of the intact fibers [21], which may vary based on composite

constituents[22]–[24]. In all composite failure, fiber failure exhibits high energy level than debonding and micro-fiber pullout [25].

Thermography is another way to quantify the damages in the composite laminate by measuring the thermal signature through active or passive mode[26] . Infrared thermography has been used as a non-destructive way of defect analysis by monitoring the surface temperature of the damaged/undamaged samples. It was observed that, after an initial drop in temperature, there exists a rise in temperature until the end of the loading cycle with visible hot spots because of irreversible damages occurring at the fiber and matrix interface leading to debonding failure (D/D) [27]. The surface temperature was the factor to find the endurance limit of flexural fatigue of unidirectional and random fiber glass-epoxy composite (Vf =70%, R = -1) [6] and recorded 1.3 times higher temperature in random fiber composite than unidirectional composite, attributed to the presence of large volume fiber discontinuity defects [28].

Depending on inherent heat generation on loading, the specimen surface can have localized as hot/cold zones [29]. In active mode thermography, the through-thickness heat conductivity of the test specimen was the property of interest on exposing to heat source. The observed drop in thermal conductivity exhibits induced material discontinuity because of the aforementioned defects and the same can be analyzed in terms of differences in heat conduction [30].

The thermal signature of fatigue-loaded (R= 0.1) CFRP samples due to notch-induced stress concentration have been captured and on mapping the temperature rise of hot zones offers a quicker way to determine the fatigue limit by NDT [31]. A similar trend of rising in temperature was recorded with in-situ impact-loaded composite thus substantiating the occurrence of damage on the structure[32] [33].

Heat dissipation measurement is one of the active IR thermography methods, which observes the dissipation pattern exhibited by the specimens on excitation. This has been tried in the analysis of damage on fatigue-loaded samples subjected to thermal excitation by halogen lamp [34], [35]. The dissipation rate remains stable for a particular stress level and increases above showing a threshold load or fatigue limit level for the chosen test specimen. This can be further extended to quantify the damage by a dissipation variable 'D' = 1- [T (@ zero stress) / T (@ applied stress)] [34]. Zacharia et al. (2012) [36] have experimented the possibility of determining the transverse thermal diffusivity of CFRP composite shells under ambient conditions. The diffusivity of the test specimens is calculated by Parker's, Cowan, Clark & Taylor's rule. The lateral conduction loss and aspect ratio of the test specimen are identified as crucial factors in the test.

Understanding the ability of NDT in characterizing the composite damage, both AE and active step heat thermography are employed in this work. The chosen GFRP composites are subjected to cyclic loading of varying frequency and load cycles. To characterize the load-induced damages, the AE outcomes in terms of frequency and number of events were measured during the flexural testing. Additionally, step heat thermography analysis was also done on the cyclically loaded specimens and the heat conduction was quantified in terms of temperature difference. In thermography tests, heat loss by convection, and radiation are considered negligible than conduction heat transfer. The heat transfer results were in good correlation with AE. The observed AE and thermography damage characteristic of the specimen reveals the significant role of fiber orientation and its volume fraction in the cyclic load-induced damage progression in FRPs.

2. Materials and Methodology

The specimens for the experiment were cut from the laminate are prepared using unidirectional glass fiber roving of 1100 GSM with denier polyester thread and epoxy matrix (LY556) with hardener (HY 995). Two types of laminate configuration with fiber orientation A= 0/30/60/0 and B= 0/90/90/0 are prepared by the hand-lay method (Fig.1). The fiber volume fraction was maintained at 1= 25% and 2= 32% for both the lay-up sequence, the laminates are configured as A1, A2, B1, and B2.

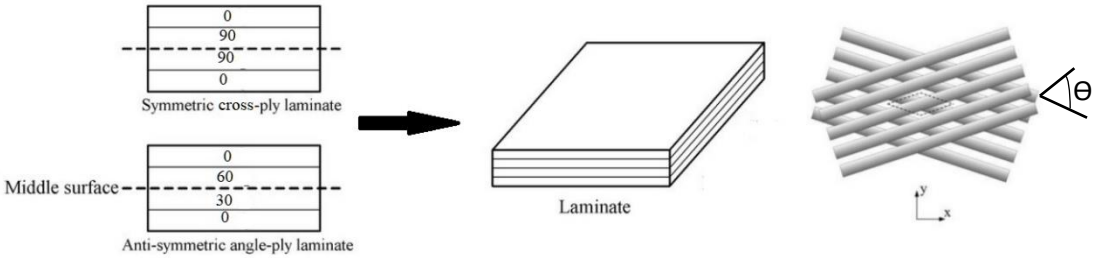

Figure 1. Illustration of fiber interaction angle in the laminate Lay -up sequence

2.1 Cyclic Loading

From the prepared laminate, specimens were cut as per ASTM D 790 suiting three-point bend test as in Fig. 2. The objective of the study is to examine the cyclic load-induced damage in the composite laminate with varying fiber orientation by AE and thermography methods. To do so, the sample dimensions are fixed in such a way to support cyclic loading followed by AE monitored flexural test and active thermography. This is exhibited in Fig. 2 a, with specimen length 150 mm, width 10 mm and thickness 4mm/5mm and also showing clamping area and loading area at which cyclic load is applied (Fig. 2 b).

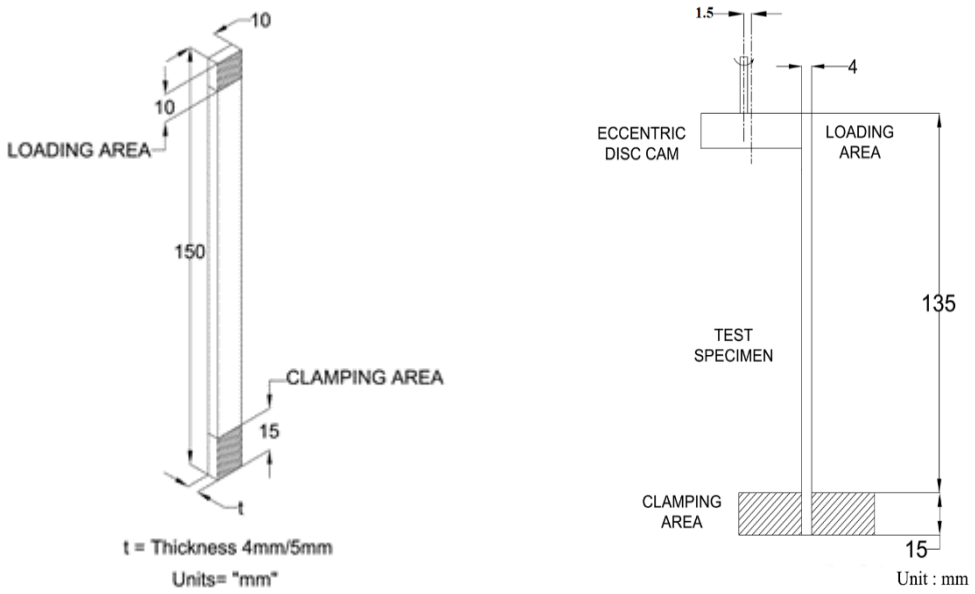

Figure 2. Illustration of a) Specimen exhibiting various areas used during cyclic loading along with dimensions suiting standard ASTM D 790 and b) Cyclic Loading by an eccentric disc

In this experiment, cyclic load was applied using an eccentric disc with an eccentricity of 1.5 mm (Fig. 1 b) for a fixed number of cycles 11,22,33,44 x 10^3 at frequencies 2.6, 4.6, 8.6 Hz. For the understanding of the reader, the specimens are named as 'virgin' before loading and 'cyclic loaded' after exposure to cyclic load. Both virgin and cyclic loaded specimens are subjected to AE monitored three-point bend test and active thermography.

2.2 Acoustic Emission monitored three-point bend test.

AE is a transient elastic wave generated by the rapid release of energy within the material under stress. The emitted waves (mostly of low amplitude and high frequency) are recorded by the piezoelectric transducers that are fixed on the surface of the component under test. The internal changes taking place in the material under study during the test are recorded as AE activities like energy, counts, and frequency. The number of AE activity signals recorded during the analysis is of paramount importance in evaluating the structural intactness. Acoustic emission (AE) [ASTM E 2076-00] monitored three-point bend test [ASTM D 790] was done to study the AE and flexural characteristics of specimens (Fig. 3). Table. 1 illustrates the AE test parameters considered for the test.

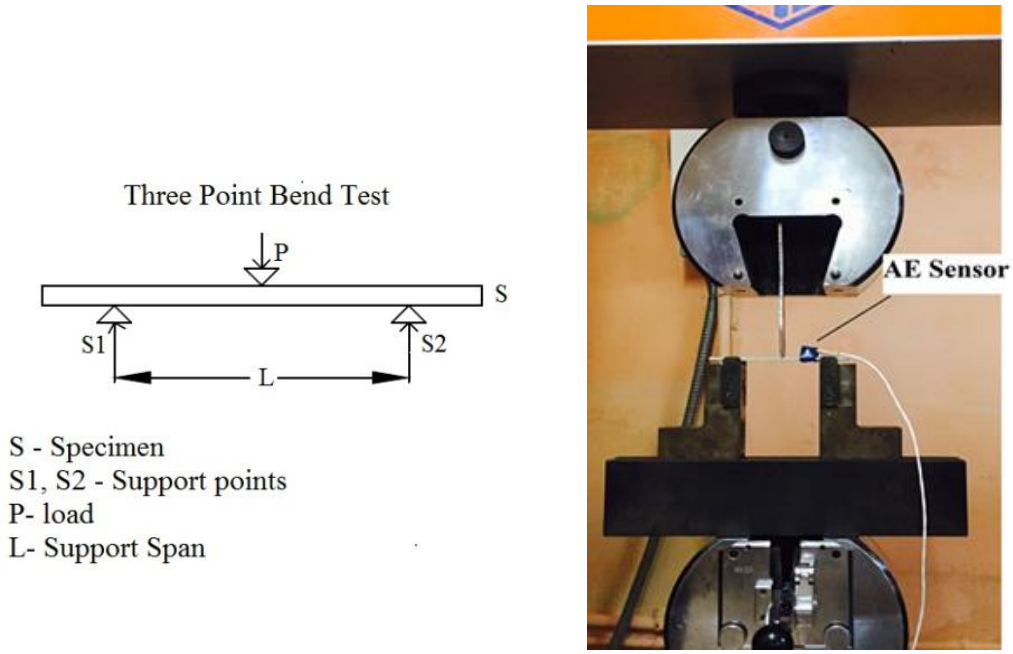

Figure 3. Flexural property evaluation by AE monitored three-point bend test

Table 1 AE Signal Characteristics, Resolution and Range (Source: *Physical Acoustics Corporation, Singapore)*

Signal Characteristics	Resolution	Unit	Range
Absolute (True) Energy	1 count	9.31×10^{-16} Joules	2.61×10^{-8} Joules
Amplitude	1dB	1dB	10-100 dB
Rise Time	1µsec	Micro sec	0-65.5 msec
Duration	1µsec	Micro sec	0-65,535 msec
Count to Peak	1 count	Counts	0-32,768 counts
Peak Frequency	1kHz	1kHz	1kHz-2100kHz
Hit Definition, Hit Lockout and Peak Definition Time	2µsec	µsec	40 µsec- 130 µsec

The flexural modulus of the test specimens was obtained by substituting the three-point bend test data in the equation. 1

$$E = \frac{mL^3}{4bd^3} \qquad \text{Eq. 1}$$

E= Flexural Modulus (kN/mm^2), m=Slope of load deflection curve of Three Point Bend test b= Specimen width =10mm, d = Specimen thickness = 4 (or) 5 mm, L= Span length of the specimen =100 mm.

2.3 Thermography Examination

Thermography is a thermal non-destructive technique to quantify the state of the composite structure in terms of matrix cracks, delamination/ debonding, and fiber failure. As in the AE evaluation, both virgin and cyclic loaded specimens were subjected to thermography examination. Step heat thermography is an active method [37], [38], in which the heat transmitted by the sample and the measured temperature difference are used to understand the intactness and internal defects[39]. An experimental set-up as shown in Fig. 4 was used to measure the top surface temperature of the specimen by IR thermometer. The surface temperature was measured at fixed locations between clamping and loading area (Fig. 4b) after attaining subsurface steady-state at specific time intervals.

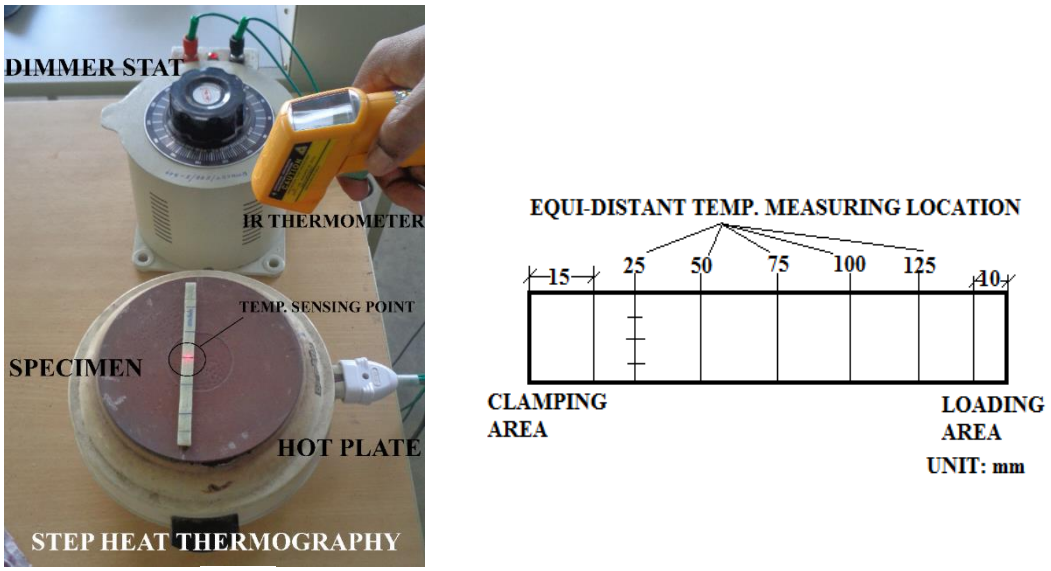

(a) (b)

Figure 4. Step heat thermography a) Experimental set-up with controllable heat source and non- contact IR temperature sensor b) Temperature measuring location between clamping and loading area.

The heat loss can be measured using the relation[40] ,

$$\boldsymbol{Q = \frac{\Delta T}{R}} \qquad \text{Eq. 2}$$

Q = Heat Loss, ΔT = Temperature difference, R = Internal resistance = $\frac{L}{KA}$, L= Length along heat flow direction = Specimen Thickness, K = Thermal conductivity of the specimen.

Thermal conductivity of the composite specimens are obtained using rules of mixture relation (Eq. 3) as follows,

$$\boldsymbol{K = (1 - V_f)K_m + V_f K_f} \qquad Eq.3$$

V_f = Fiber volume fraction, K_m = Thermal conductivity of the epoxy matrix = 0.363 W/mK, K_f = Thermal conductivity glass fiber = 1.04 W/mK.

As the specimen thickness (4mm and 5 mm) and thermal conductivity (K = 0.58 W/mK for V_f = 32% and K= 0.53 W/mK for V_f =25%) are constant, thus the heat loss by the

composite specimen is directly proportional to ΔT, i.e., the temperature difference between the top and bottom surface. Here, the specimen is kept on the hot plate whose temperature is maintained at 100 ^{0} C during observation. The magnitude of ΔT would certainly represent the degree of internal damages in the structure that might have been created by the manufacturing process and/or during loading[41]. The temperature on the top surface of the specimens is measured at five equidistant lines between loading and clamping area (Fig. 3 b). At each line, three equidistant points are marked and an average of the three temperatures at those points was taken as line temperature.

3. Result and Discussion

The behavior of the composite laminate on exposure to cyclic loading was evaluated in terms of flexural modulus, AE events/peak frequency, and thermography is presented in the following section.

3.1 Flexural Modulus response

The chosen laminate configurations were exposed to cyclic load with frequencies 2.6, 4.6 and 8.6 Hz up to a maximum of $44x10^3$ cycles (Fig 5 and 6). The imposed cyclic loading induces matrix crazing and the subsequent propagation is mostly confined by the reinforcing fiber, thereby indicating the onset of crack arresting mechanism. This phenomenon is reflected as a marginal variation of the flexural modulus of the laminate exposed at frequencies 2.6 Hz and 4.6 Hz (Fig. 5a). Also, it is seen that, around the $44x10^3$ cycle, the effect of loading frequency is almost nil. However, with 8.6 Hz, A1 laminate exhibits an initial drop followed by rising in flexural modulus values which is well below the virgin laminate.

The variation of flexural modulus with the frequency of cyclic load in the case of symmetrical lay-up B1 (0/90/90/0) is illustrated in Figure 5 b. It is seen that, exhibits a small reduction in the flexural modulus after $11x10^3$ cycles and retains its value up to around $44x10^3$ cycles. It is noted that B1 laminate has almost shown identical variation with the frequencies 4.6 Hz and 8.6 Hz up to $33x10^3$ cycles. It is seen that B1 shows a considerable drop in flexural modulus after $33x10^3$ cycles, especially for the 8.6Hz frequency. With increasing matrix-fiber orientation angle in B1, the structural response and consequent damage control tolerance are found to be weak for lower loading frequency (2.6 Hz) than others (4.6 Hz and 8.6 Hz).

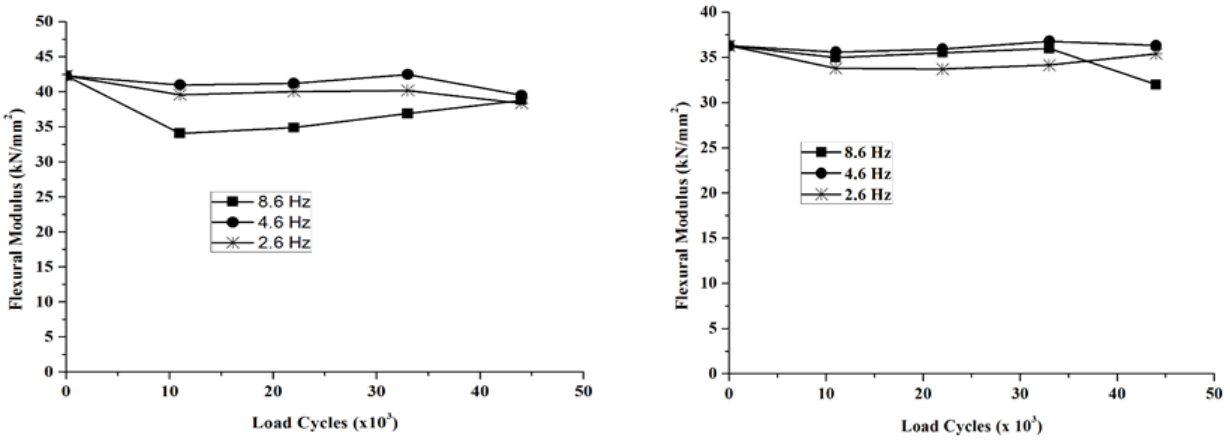

(a) (b)

Figure 5. Flexural Modulus of cyclic loaded samples V_f =32% a) A1 - 0/30/060/0 b) B1- 0/90/90/0

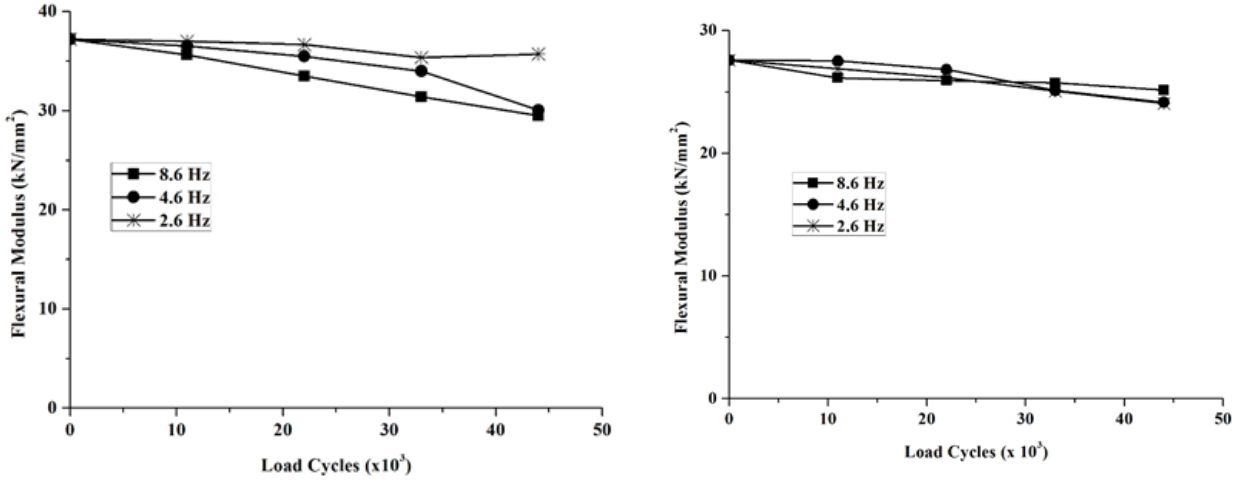

(a) (b)

Figure 6. Flexural Modulus of cyclic loaded samples V_f =25% a) A2 - 0/30/060/0 b) B2- 0/90/90/0

Sl. No.	Loading Frequency	Load Cycle X10³	Flexural Modulus of 0/90/90/0 Laminate			
			Actual (kN/mm²)			% variation with respect to 25 % V_f
			Type A	Type B	Type C	Type C
1	8.6 Hz	11	35	26.15	27.6	5.3
2		22	35.54	25.92	27	4
3		33	36	25.74	26.63	3.3
4		44	32	25.14	25.43	1.1
1	4.6 Hz	11	35.6	27.54	28.13	2.0
2		22	35.95	26.84	27.61	2.8
3		33	36.8	25.12	26.13	3.8
4		44	36.33	24.15	25.35	4.7

1	2.6 Hz	11	33.8	26.89	28.32	5.0
2		22	33.72	26.17	28.3	7.5
3		33	34.16	25.06	27	7.2
4		44	35.41	24.05	27.15	11.4

Sl. No.	**Loading Frequency**	**Load Cycle X10^3**	**Flexural Modulus of 0/30/60/0 Laminate**			
			Actual (kN/mm^2)			**% variation with respect to 25 % V_f**
			Type A	**Type B**	**Type C**	**Type C**
1	8.6 Hz	11	34.1	35.64	37.05	3.8
2		22	34.9	33.5	34.25	2.1
3		33	36.92	31.4	31.95	1.7
4		44	38.8	29.5	30.53	3.3
2	4.6 Hz	11	41	38.54	39.42	2.2
2		22	41.24	35.5	36.15	1.8
3		33	42.5	34	34.78	2.2
4		44	39.52	30.05	31.05	3.2
1	2.6 Hz	11	39.6	38.02	39.76	4.3
2		22	40.07	37.66	37.92	0.7
3		33	40.2	35.37	36.58	3.3
4		44	38.4	35.72	36.52	2.2

Typical observed variation of flexural modulus of A2 (V_f = 25%) laminated exposed to cyclic loading is illustrated in Fig. 6a. It is seen that, cyclic loading of laminate with a lower frequency of 2.6 Hz results in sustaining its modulus up to around 44x10^3 cycle, while a drop in modulus can be seen in 4.6 Hz and 8.6 Hz frequencies. This is in contrast to the observation on A1 laminate (Figure. 5 a) and exhibits a higher energy absorption. With higher resin/matrix content and increased matrix–reinforcement interaction angle, the resin/ matrix has a dominant influence on loading frequency. With increasing loading frequency (4.6 Hz and 8.6 Hz), the resistance offered by fiber- matrix reduces leading to lower-order flexural modulus.

The B2 laminate with a lower fiber volume fraction (25%) (Fig. 6 b) exhibits a marginal reduction in the modulus with all frequencies around 22x10^3 load cycles. This is in contrast to the observation with B1 (Fig. 5 b), wherein with 4.6 Hz and 8.6 Hz frequencies, the composite laminate with V_f =32% sustain its modulus up to around 33x10^3 cycles. With increasing matrix – reinforcement interaction angle, matrix the dominant response would be realised. With 90^0 orientations, the reinforcement in the matrix is prone to fracture, and as such the composite may not experience an effective crack arresting mechanism. Thus, in the case of B2 laminate, with a reduced volume fraction of reinforcement, not much of a crack arresting mechanism was possible. The observed drop in modulus in the early phase of cyclic loading,

followed by subsequent recovery in the case of A2 laminate is mostly absent with B2 Type laminate.

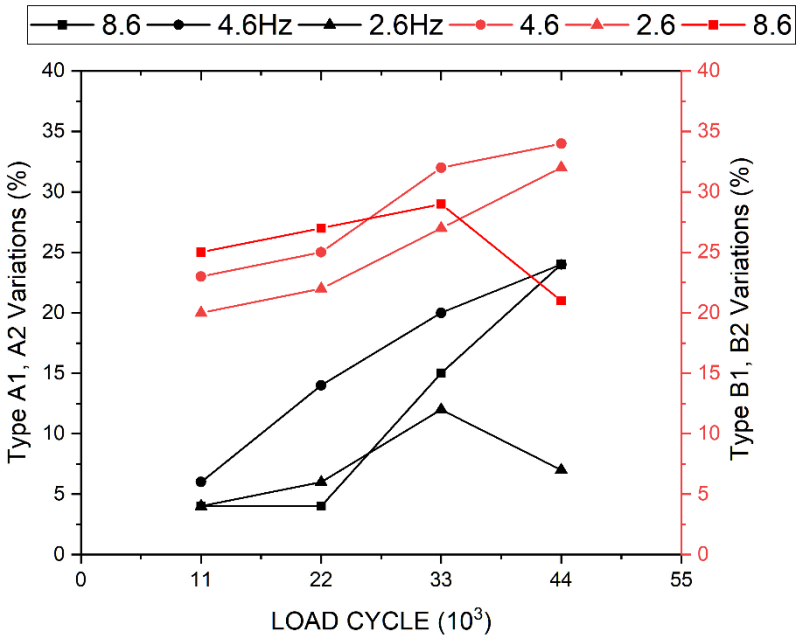

Figure 7. Flexural Modulus variation among cyclic loaded A1&A2 and B1&B2 Laminates

The variations in the performance of cyclic loaded laminates of varying V_f is shown in Fig.7. It is observed that, laminate with a higher fiber interaction angle within the lay-up sequence (Type B- 0/90/90/0) has higher variations in the flexural modulus of cyclically loaded composites than the laminate with a lower fiber interaction angle (Type A – 0/30/60/0). However, the loading frequency 4.6 Hz has presented overall higher variations in Type A and only for higher loading cycles in Type B. Thus, laminate configuration with fiber volume fraction range V_f = 32 - 25%, loading frequency 4.6 Hz can be considered as a threshold value to mark notable changes in the flexural responses. Fig.8 illustrates the damage mechanisms in the respective laminate A and B during three point flexural tests.

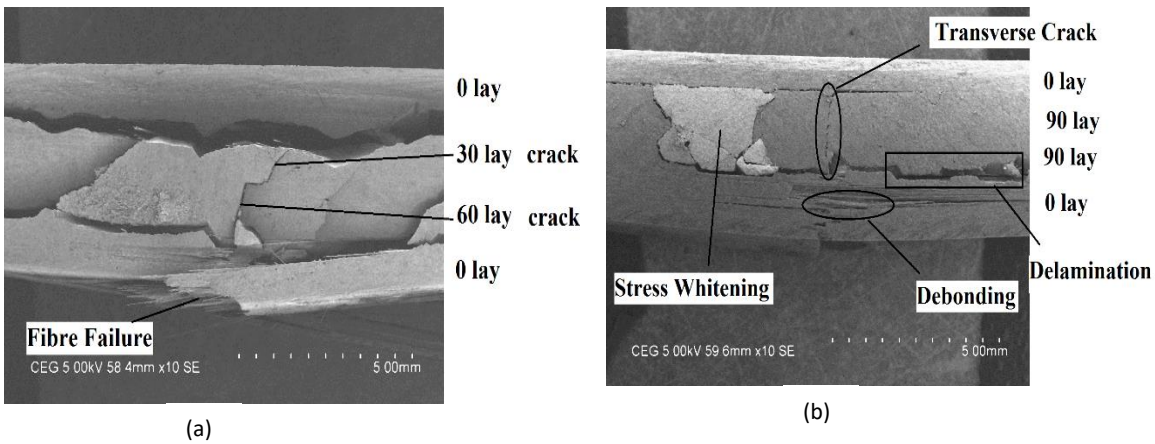

Figure 8. SEM of Flexural tested Laminate a) A1 and b) B1

3.2 Acoustic Emission (AE) responses

In the present analysis, Energy level, Counts and Peak frequency of the AE events occurred during flexural test of the laminates before (virgin) and after cyclic loaded laminates were observed and quantified to characterize their behaviors.

3.2.1 AE event energy and duration

On observing Fig. 9 a, the maximum duration of the AE event is up to $5x10^4$ μsec. Majority of the events are with energy value less than 100 μvolt-sec and up to 10^4 μsec and few events are crossing the more than 200 μ volt-sec. Thus, the total energy of the AE event of virgin A1 laminate is 7370 μvolt-sec. The short time span of AE event occurrences and the energy directly depicts the strength of the laminate and be a factor of comparison with virgin laminates.

The energy distribution of the virgin B1 laminate is given in Fig. 9 b. It is observed that the duration for AE event completion is with a maximum duration of 2000 μsec. Though more of the events are below 200 μvolt-sec, the total energy of the AE event is 6213 μvolt-sec. The smaller energy release compared to the A1 laminate and earlier emission could be attributed to the less effective orthogonal orientation crack arresting and higher energy absorption.

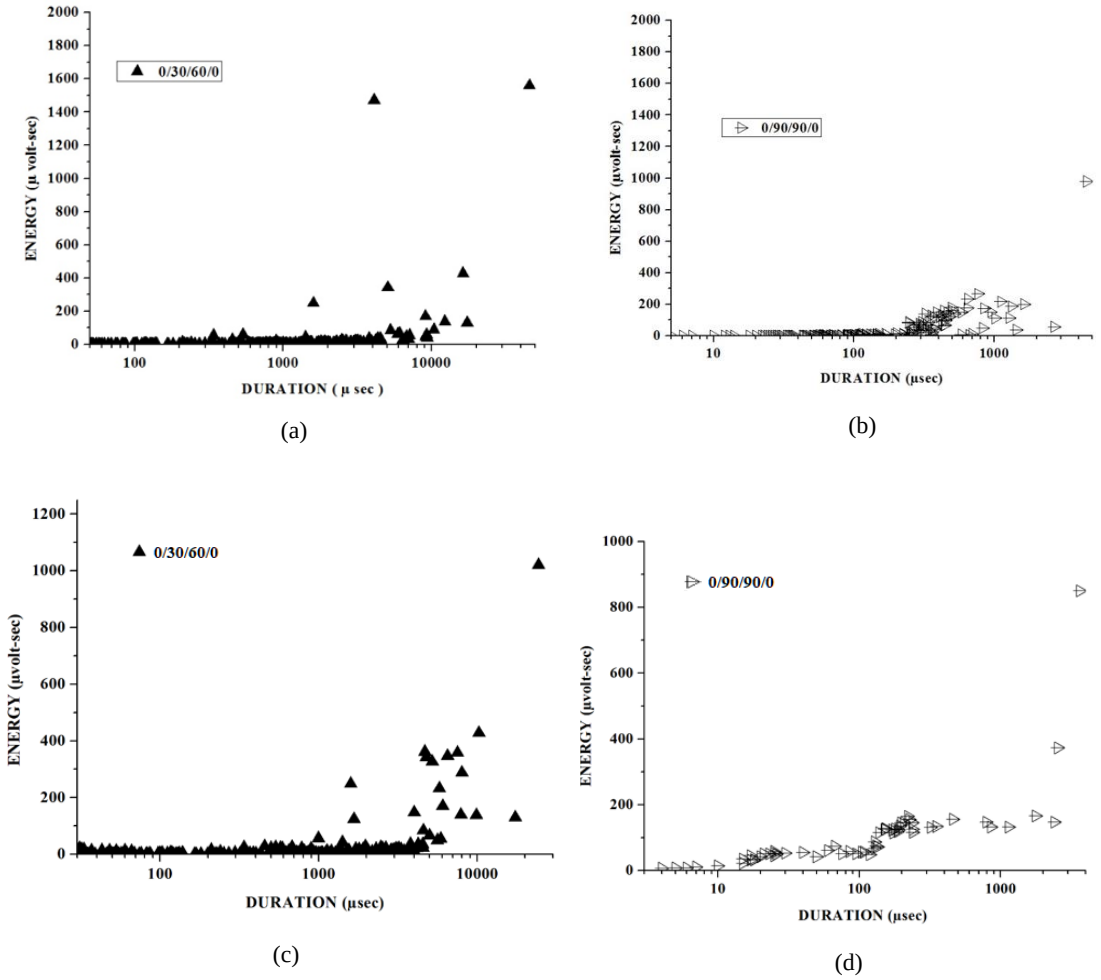

Figure 9. AE Energy Vs Duration of a) A1, b) B1, c) A2 and d) B2 Laminate

The energy distribution of A2 laminate is given in the Fig. 9 c. The observation shows that, majority of AE events are with lower energy level (< 100 μvolt-sec) and appears denser up-to 5000 μsec. Only few events occurred after 5000 μsec are with energy > 1000 μvolt-sec. The total energy of the AE event distributed over a span of 24350 μsec is 7880 μvolt-sec, which slightly higher than its counterpart A1 (7370 μvolt-sec). The higher AE event energy of A2 establishes the scope of the material to undergo sufficient internal changes to accommodate the applied load. However, the sustainability of the laminate to the load is quantified by the event duration.

Fig. 9 d, illustrates the energy distribution of virgin B2 laminate. It is observed that, the energy values of the AE events gradually rise up to 100 μvolt-sec around 100 μsec. Beyond that, the steady AE events with an energy value of maximum 200 μvolt-sec are seen up to around 2000 μsec. Though the total energy of AE events of B2 is 6257 μvolt-sec extended for a duration of 3647 μsec and the trend of the events presented by B2 is entirely different from the B1 attributed to the change in V_f. Thus, it can be understood that, with the rise in matrix content, the number of high energy events may increase during the initial period of testing.

The typically monitored AE energy of the A1 laminate after cyclic load is given in the Fig. 10a. The total AE events of A1 laminate exhibits 5873 μvolt sec of energy with a duration

of $23x10^3$ μsec. In comparison with virgin A1 (Fig. 8a), cyclic loaded A2 laminate has more AE events in the energy range 200 μvolt sec – 979 μvolt sec attributed to the fibre failure as majority of matrix crazing would have occurred during cyclic loading. The AE energy of cyclic loaded B1 is illustrated in the Fig. 10b. It is seen that, the total energy value (B1 = 4774 μvolt sec) and the duration of the event are reduced when compared with that of respective virgin laminates. The influence of the 90^0-fibre orientation is exhibited by the occurrence of low energy AE events around 300 – 1000 μsec.

Fig. 10c, illustrate the energy distribution of A2 laminate after exposure to $44x10^3$ load cycles at 4.6 Hz of loading frequency. The flexural test of the A2 laminate after cyclic load exhibits AE events which comprise the majority of higher energy events and fewer lower-order events. This sort of energy distribution explicitly shows the occurrence of lower-order damage during cyclic loading and the retained higher-order events during the flexural test (Three-point bend test). The total energy of the A2 laminate was 6340 μvolt sec in a duration of 18767 μsec. The AE energy response of the cyclic loaded B2 laminate obtained during the flexural test is illustrated in Fig. 10d. The total energy of B2 laminate is 5514 μvolt sec in a duration of 2246 μsec. Similar to the other laminates, most of the events are high energy events with sparse distribution/ absence of low-energy events.

Table 2. Changes in the AE energy of virgin and cyclic loaded laminates

Laminate Configuration	Total AE Energy μvolt sec		
	Virgin Laminate	Cyclic Loaded Laminate ($44x10^3$, 4.6 Hz)	% Drop
A1	7464	5873	30.74
B1	6213	4774	23.16
A2	7880	6640	15.73
B2	6257	5514	11.87

The AE energy response of cyclic loaded ($44x\ 10^3$ load cycle and 4.6 Hz) Type A and B laminates obtained during the three-point bend test is given in Table 2. It is observed that the percentage drop of A1 is maximum after exposure to the cyclic load. Whereas, the Type A2 laminates exhibit a lesser drop in AE energy. The AE energy of the cyclic loaded laminate Type B1 exhibits a maximum drop of around 23%, which comparatively lower value than the Type A laminate for the same loading conditions. On exposing the laminate to cyclic load, the composite structure experiences damages of varying order based on the type of loading, and the induced damage certainly reduces the energy capacity of the laminate. The overall variation in the AE energies between Type A and B is the significant role of fiber orientation interaction angle. Whereas, in Type B laminate the drop in energy level is minimum because of the presence of more energy-absorbing site matrix/resin in the lay-up sequence.

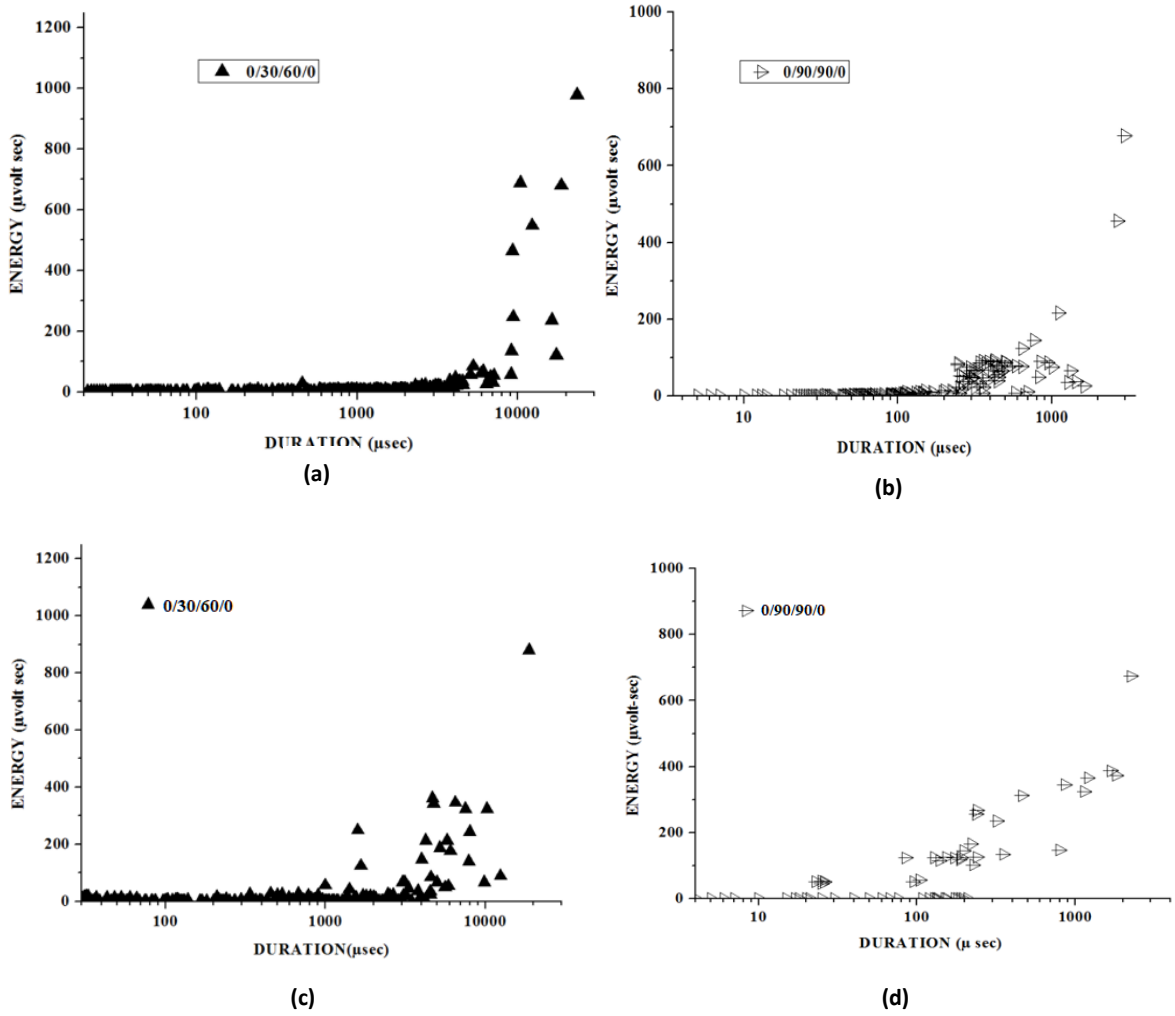

Figure 10. AE Energy Vs Duration of cyclic loaded laminates (44x 10^3 cycles at 4.6 Hz) a) A1, b) B1, c) A2 and d) B2 Laminate

3.2.2 AE event peak frequency and counts

As mentioned earlier, AE event peak frequency and event counts are the other associated parameters during the AE monitored flexural tests on the specimens. Fig.11 a, illustrates the AE peak frequency and count of virgin A1 laminate. It is seen that the clustering of AE events was more in the matrix crazing/cracking than the delamination/debonding and fiber failure zone[42]. The peak frequency zone of matrix crazing was very narrow in the range of 75 kHz-110 kHz. Whereas the delamination/ debonding zone is spread in a wider range of 110 kHz – 225 kHz and the fiber failure is in the range 290 kHz- 380 kHz[20]. In A1 laminate, the core 30/60 fiber layer propagate interface damage initiated by the matrix crack as observed by the wider AE distribution events in the mid zone. The existence of predominant matrix crazing and interface damage depletes the effect of fiber reinforcement in the structure which is observed as sparse AE peak frequency distribution in the fiber failure zone. On observing the AE count, A1 laminate has a maximum of 3250 counts around $30x10^4$ µsec

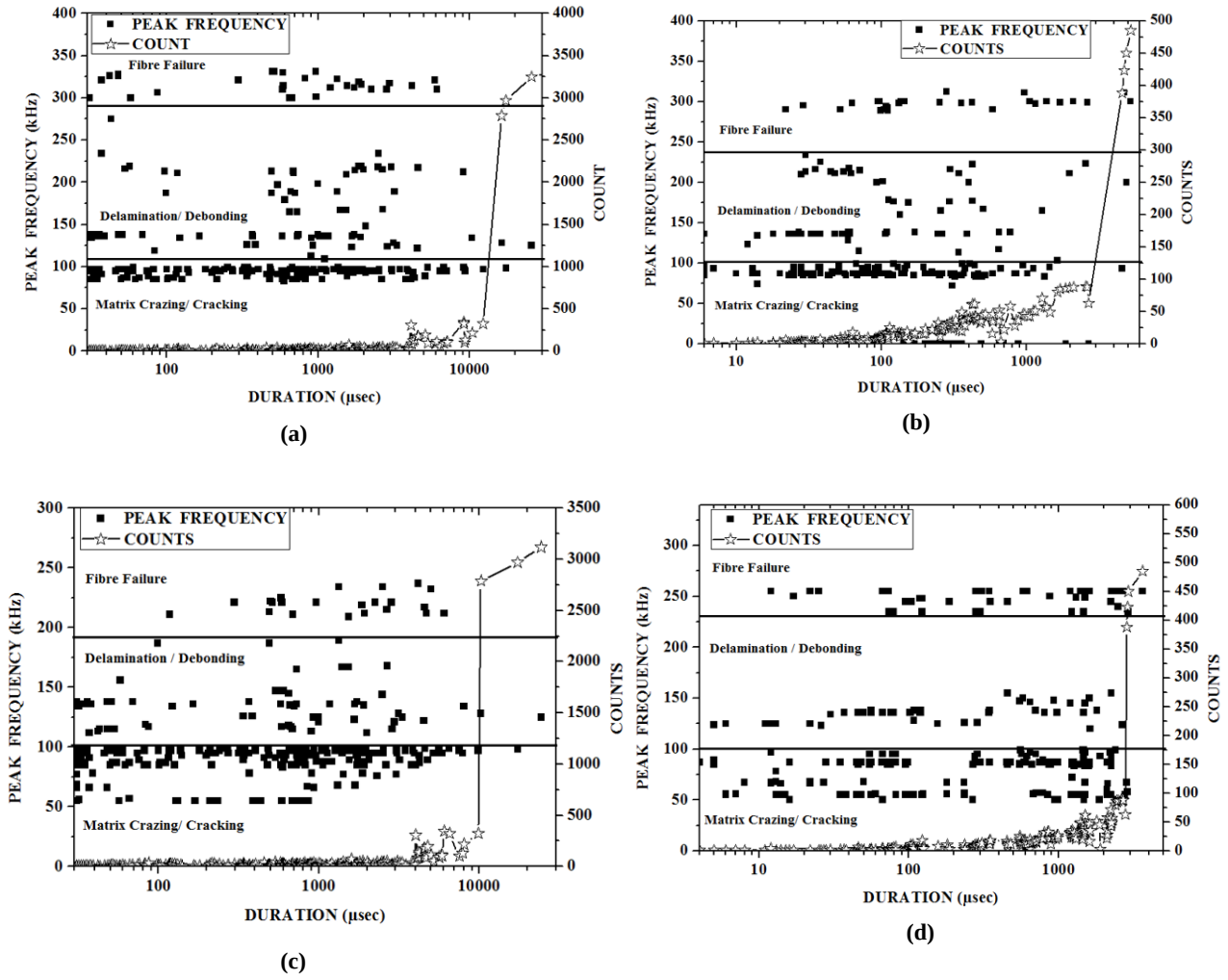

Figure 11. AE Peak Frequency and Counts of Virgin Laminates a) A1, b) B1, c) A2 and D) B2

Typical AE event peak frequency and count of B1 laminate is shown in the Fig. 11 b. The maximum clustering of peak frequency is seen in the lower frequency range 75 kHz – 100 kHz exhibiting the occurrence of matrix crazing/ cracking. The interface damage in the B1 laminate is in the frequency range of 100 kHz – 240 kHz with the distribution of AE events up to around 10^3 µsec. The peak frequency for fiber failure is in the range of 275 kHz- 290 kHz and the maximum count is 525.

Fig. 11 c, illustrates the AE parameter response of the A2 laminate. More clustering of AE events was seen in the matrix/resin crazing zone with a frequency range of 50 kHz – 100 kHz. The wider occurrence of matrix crazing is attributed to a higher resin volume fraction (V_r= 75%). Whereas, the interface damage (delamination/debonding) and fiber failure are in the peak frequency range of 110 kHz- 175 kHz and 200 kHz- 245 kHz respectively. The maximum event count is 3120 distributed over a period of 24x10^3 µsec. The virgin cross-ply laminate Type B2 presents a peak frequency range of 50-100 kHz, 120-155 kHz, and 200-255 kHz in the matrix, delamination, and fiber failure region respectively with a maximum AE count of 485 in 3647 µsec (Fig. 11 d).

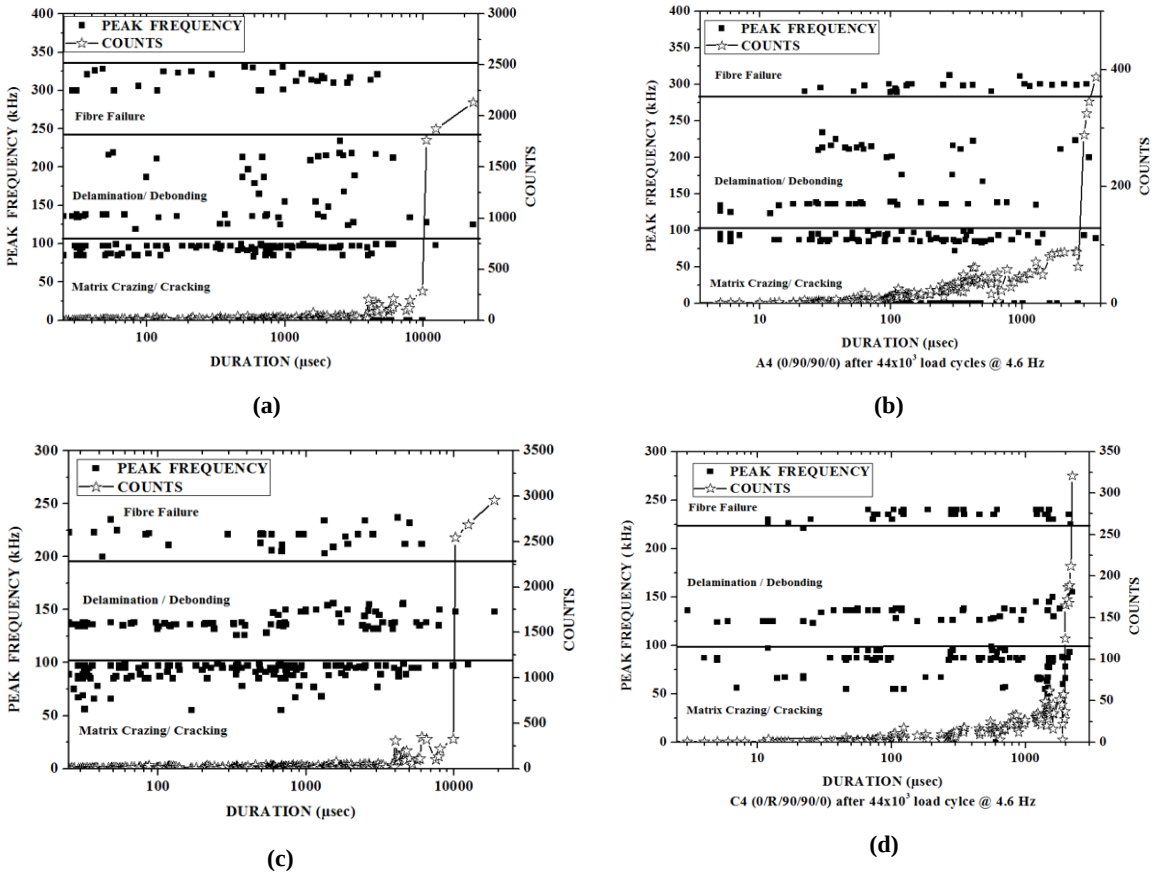

Figure 12. AE Peak frequency distribution and count of Cyclic loaded (44x 10^3 cycles at 4.6 Hz) Type a) A1, b) B1, c) A2 and d) B2 Laminate

Table. 3 AE Peak Frequency, Maximum Count and Duration of Type A and B Laminate

Laminate Type	Virgin/ Loaded	Peak Frequency (kHz)			Max. Counts	Duration µsec
		Matrix Crazing	Delamination/ debonding	Fibre failure		
A1	Virgin	75-110	110-225	290-380	3250	45,703
	Loaded	50-100	100-245	290-330	2134	23,014
B1	Virgin	75-100	100-240	275-310	525	5200
	Loaded	75-100	100-240	260-305	395	3657
A2	Virgin	50-100	110-175	200-245	3120	24,359
	Loaded	50-100	120-160	210-235	2956	18,767
B2	Virgin	50-100	120-155	225-260	485	3647
	Loaded	50-100	115-155	220-240	331	2246

The AE response of the cyclic loaded Type A laminate in-terms of peak frequency and counts is given in Fig. 12a and Table.3. It is observed that, the peak frequency range of cyclic loaded laminate in the damage modes matrix cracking (MC), delamination/debonding (D/D) and fibre failure (FF) are more or less the same as that of virgin laminate, whereas the maximum counts and duration of the AE events are reduced because of the damage induced by the cyclic loading. This sort of AE event count variations (34.33%) could quantify the influence of lay-up sequence in dynamic loading condition.

Type B 1 laminate (Table. 3 and Fig. 12 b), the peak frequency ranges for MC, D/D and FF after exposing it to cyclic load is resembling the virgin Type B1, however, there exists a drastic drop in the number of events and the duration. A variation of 24.76% was noticed between virgin and loaded Type B1 laminates. The peak frequency of the AE events of Type A2 and B2 laminate shows a marginal deviation in D/D and FF only and not much in MC, whereas the number of events shows a variation of 5.26% and 33.81% respectively.

Although the peak frequency for various damage phenomena was marginally similar, the AE counts and the duration acts were found to have drastic variations. The reduced AE count variation (5.26%) in A2 is because of significant energy dissipation and retained intactness of fiber, attributed to higher resin/ matrix content in the laminate (Fig. 12c). Whereas, in the addition of resin in B2 laminate is not much significant (with a variation of 33.81%) because of orthogonal fiber orientation with a higher fiber interaction angle in the lay-up sequence (Fig. 12d).

3.3 Temperature differences

The observed ΔT of virgin and cyclic loaded laminates were measured using IR thermometer starting from the fixed end and plotted (Fig. 13). A1 laminate, exhibits a varying drop in the ΔT with respect to loading frequencies. 4.6 Hz loading frequency has lower and 8.6 Hz has higher ΔT variations than virgin samples (Fig. 12 a).

The ΔT variation of B1 laminate is illustrated in Fig. 13 (b). The effect of loading frequency on ΔT variation is similar to that of A1 with marginal drop. 4.6 Hz loading frequency offers minimum ΔT variation exhibiting the possible changes in the composite system with a rise in flexural modulus as mentioned in section 3.1. Here also, the magnitude of ΔT is comparatively higher than A1, indicting the possible damages induced by the cyclic load in cross-ply laminate.

Fig. 13 c illustrates the ΔT variation of A2 laminate. It is seen that the trend of A2 exhibiting higher-order ΔT for virgin and lower order value for the cyclic loaded specimens. Also, the magnitude variation of ΔT among loading frequencies may be because of load-induced changes in the matrix system which requires intrinsic evaluation like active in-situ thermography. The illustrated ΔT variation of B2 laminate (Fig. 13 d) exhibits a similar trend as that of A2 laminate with marginal magnitude variation for specimens exposed to cyclic loading at 2.6 Hz and 4.6 Hz and higher ΔT value for 8.6 Hz loading.

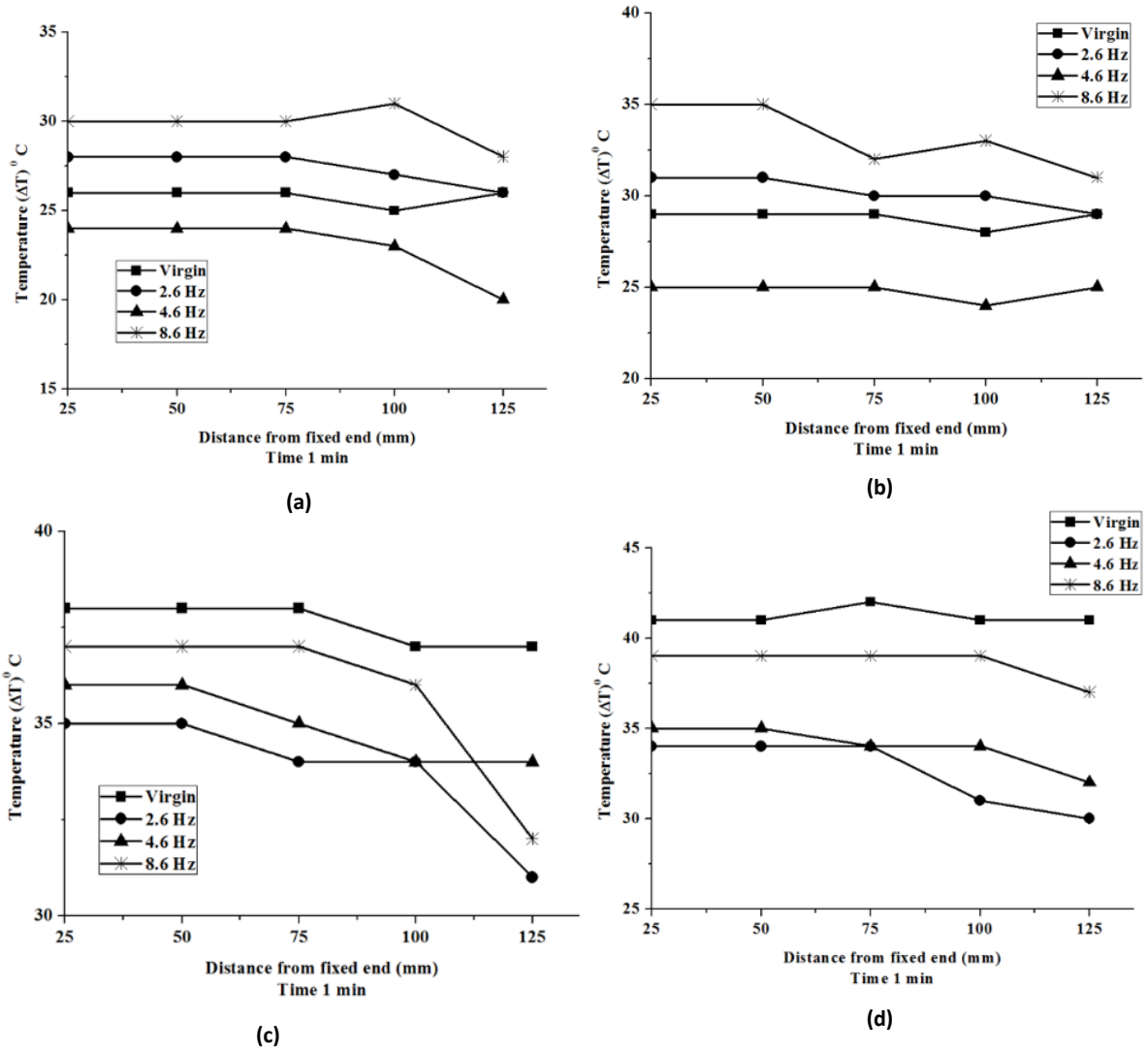

Figure. 13 Temperature difference Plot (ΔT) of Type a) A1, b) B1, c) A2 and d) B2 laminate

4. Conclusions

The GFRP composite laminate with varying fiber orientations (0/30/60/0 and 0/90/90/0) was exposed to cyclic loading up to around 44 x 10^3 cycles with 2.6 Hz, 4.6 Hz, and 8.6 Hz as loading frequencies. The response of the GFRP laminates was evaluated through AE monitored three-point bend tests and step heat thermography. The observed parameters in the experiments were Flexural modulus, Acoustic energy, peak frequency and acoustic event counts in AE monitored flexural test, and temperature difference in step heat thermography.

The cyclic loading of moderate frequency (4.6Hz) contributes to the better flexural performance of GFRP with reduced fiber interaction angle within the lay-up than higher and lower frequency (8.6 and 2.6 Hz). Whereas, for GFRP higher fiber interaction angle (0/90/90/0) lower loading frequency (2.6Hz) was found to retain the flexural properties. The effect of loading frequency for higher flexural performance has a shift from moderate (4.6 Hz) to lower (2.6 Hz) with drop-in V_f. Thus, composite with lower V_f is better suitable for lower loading frequency for better performance. Also, the variation in flexural modulus is directly

proportional to the fiber interaction angle within the lay-up sequence. The laminate configuration with fiber volume fraction range V_f = 32 - 25%, loading frequency 4.6 Hz can be considered as a threshold value to mark notable changes in the flexural responses.

The AE monitored flexural damage phenomenon is characterized as Matrix cracking / crazing (MC), Delamination / debonding (D/D), and Fiber Failure (FF) with respective peak frequencies and cumulative counts of AE events. The peak frequency ranges for the above damage phenomenon for both laminates were 50-100, 110-230, 245-380 kHz with variations in AE event count and duration with regard to the resistance offered. The drop-in fiber volume fraction is significant in laminate with lower fiber interaction to offer minimum variation in AE activity exhibiting matrix dominant behavior which is missing in laminate with higher fiber interaction angle.

The step heat thermography of cyclically loaded higher V_f composites exhibits minimum ΔT for moderate loading frequency, whereas with lower V_f the imposed cyclic loading encounters drop in ΔT well below the virgin sample. This warrants in-situ thermography to study dynamic changes in the fiber-matrix system.

5. References

[1] M. Kavousi Sisi, M. Shakeri, and M. Sadighi, "Dynamic response of composite laminated beams under asynchronous/repeated low-velocity impacts of multiple masses," *Composite Structures*, vol. 132, pp. 960–973, Nov. 2015, doi: 10.1016/j.compstruct.2015.06.072.

[2] A. Refahi and J. Yousefi, "ScienceDirect Characterization of residual strength in transversely loaded glass- polyester composites by acoustic emission and sentry function ƒ," *Materials Today: Proceedings*, vol. 5, no. 1, pp. 381–387, 2018, doi: 10.1016/j.matpr.2017.11.095.

[3] J. Guo, J. Wang, and C. Bian, "Cyclic tensile behavior of high strain hardening UHPC analyzed by acoustic emission techniques," *Construction and Building Materials*, vol. 267, p. 121797, 2021, doi: 10.1016/j.conbuildmat.2020.121797.

[4] Y. Wu, M. Perrin, M. Pastor, P. Casari, and X. Gong, "On the determination of acoustic emission wave propagation velocity in composite sandwich structures," *Composite Structures*, vol. 259, no. November 2020, p. 113231, 2021, doi: 10.1016/j.compstruct.2020.113231.

[5] G. Belingardi and M. P. Cavatorta, "Bending fatigue stiffness and strength degradation in carbon-glass/epoxy hybrid laminates: Cross-ply vs. angle-ply specimens," *International Journal of Fatigue*, vol. 28, no. 8, pp. 815–825, 2006, doi: 10.1016/j.ijfatigue.2005.11.009.

[6] T. J. Adam and P. Horst, "Experimental investigation of the very high cycle fatigue of GFRP [90/0]s cross-ply specimens subjected to high-frequency four-point bending," *Composites Science and Technology*, vol. 101, pp. 62–70, Sep. 2014, doi: 10.1016/j.compscitech.2014.06.023.

[7] M. M. Shokrieh and D. Rezaei, "Analysis and optimization of a composite leaf spring," vol. 60, pp. 317–325, 2003, doi: 10.1016/S0263-8223(02)00349-5.

[8] C. V. Singh and R. Talreja, “International Journal of Solids and Structures Evolution of ply cracks in multidirectional composite laminates,” *International Journal of Solids and Structures*, vol. 47, no. 10, pp. 1338–1349, 2010, doi: 10.1016/j.ijsolstr.2010.01.016.

[9] R. Sakin, I. Ay, and R. Yaman, “An investigation of bending fatigue behavior for glass-fiber reinforced polyester composite materials,” *Materials and Design*, vol. 29, no. 1, pp. 212–217, 2008, doi: 10.1016/j.matdes.2006.11.006.

[10] Md. T. A. Ansari, K. K. Singh, and M. S. Azam, “Fatigue damage analysis of fiber-reinforced polymer composites—A review,” *Journal of Reinforced Plastics and Composites*, vol. 37, no. 9, pp. 636–654, 2018, doi: 10.1177/0731684418754713.

[11] Y. Lin, C. Liu, H. Li, K. Jin, and J. Tao, “Interlaminar failure behavior of GLARE laminates under double beam five-point-bending load,” *Composite Structures*, vol. 201, pp. 79–85, Oct. 2018, doi: 10.1016/j.compstruct.2018.06.037.

[12] R. Dalai and B. C. Ray, “Failure and Fractography Studies of FRP Composites : Effects of Loading Speed and Environments Failure and Fractography Studies of FRP Composites : Effects of Loading speed and Environments,” no. July 2015, 2011.

[13] K. Naresh, K. Shankar, B. S. Rao, and R. Velmurugan, “Effect of high strain rate on glass / carbon / hybrid fi ber reinforced epoxy laminated composites,” *Composites Part B*, vol. 100, pp. 125–135, 2016, doi: 10.1016/j.compositesb.2016.06.007.

[14] Y. Ou, D. Zhu, H. Zhang, Y. Yao, B. Mobasher, and L. Huang, “Mechanical properties and failure characteristics of CFRP under intermediate strain rates and varying temperatures,” *Composites Part B*, vol. 95, pp. 123–136, 2016, doi: 10.1016/j.compositesb.2016.03.085.

[15] Oz, Fatih E., Nuri Ersoy, and Stepan V. Lomov. "In-situ damage monitoring and correlation with Acoustic Emission in CFRP composites." *In ICCM International Conferences on Composite Materials*, vol. 2017.

[16] K. Kalteremidou, D. G. Aggelis, D. van Hemelrijck, and L. Pyl, “On the use of acoustic emission to identify the dominant stress / strain component in carbon / epoxy composite materials,” *Mechanics Research Communications*, vol. 111, p. 103663, 2021, doi: 10.1016/j.mechrescom.2021.103663.

[17] K. A. Kalteremidou, D. G. Aggelis, D. van Hemelrijck, and L. Pyl, “On the use of acoustic emission to identify the dominant stress/strain component in carbon/epoxy composite materials,” *Mechanics Research Communications*, vol. 111, Jan. 2021, doi: 10.1016/j.mechrescom.2021.103663.

[18] L. Li, S. v. Lomov, and X. Yan, “Correlation of acoustic emission with optically observed damage in a glass/epoxy woven laminate under tensile loading,” *Composite Structures*, vol. 123, pp. 45–53, May 2015, doi: 10.1016/j.compstruct.2014.12.029.

[19] F. E. Oz, N. Ersoy, and S. v Lomov, “In-situ damage monitoring and correlation with Acoustic Emission in CFRP composites,” in *ICCM International Conferences on Composite Materials*, 2017, vol. 2017-August.

[20] J. Kakakasery *et al.*, “Cure cycle effect on impact resistance under elevated temperatures in carbon prepreg laminates investigated using acoustic emission,” *Composites Part B: Engineering*, vol. 75, pp. 298–306, Jun. 2015, doi: 10.1016/j.compositesb.2015.02.002.

[21] M. Saeedifar, M. Nasr, H. M. El-dessouky, and D. Freitas, “Damage assessment of NCF , 2D and 3D woven composites under compression after multiple-impact using acoustic emission,” vol. 132, no. December 2019, 2020, doi: 10.1016/j.compositesa.2020.105833.

[22] I. Emami, A. Kefal, J. Seyyed, M. Zanjani, and C. Akalin, “Experimental and numerical investigation on fracture behavior of glass / carbon fi ber hybrid composites using acoustic emission method and re fi ned zigzag theory,” *Composite Structures*, vol. 223, no. February, p. 110971, 2019, doi: 10.1016/j.compstruct.2019.110971.

[23] Xu, D., P. F. Liu, and Z. P. Chen. "Damage mode identification and singular signal detection of composite wind turbine blade using acoustic emission." *Composite Structures* 255 (2021): 112954.. doi.org/10.1016/j.compstruct.2020.112954

[24] Zhou, Wei, Peng-fei Zhang, and Yan-nan Zhang. "Acoustic emission based on cluster and sentry function to monitor tensile progressive damage of carbon fiber woven composites." *Applied Sciences* 8, no. 11 (2018): 2265. doi.org/10.3390/app8112265

[25] Q. Li, Y. Li, Z. Zhang, Z. Zhang, and L. Zhou, “Quantitative investigations on multi-layer interface debonding behaviors for sisal fiber reinforced composites using acoustic emission and finite element method,” *Composites Part B*, vol. 196, no. May, p. 108128, 2020, doi: 10.1016/j.compositesb.2020.108128.

[26] J. N. Zalameda and W. P. Winfree, “Passive Thermography Measurement of Damage Depth During Composites Load Testing,” *Frontiers in Mechanical Engineering*, vol. 7, Apr. 2021, doi: 10.3389/fmech.2021.651149.

[27] C. Colombo and L. Vergani, “Influence of delamination on fatigue properties of a fibreglass composite,” *Composite Structures*, vol. 107, no. 1, pp. 325–333, Jan. 2014, doi: 10.1016/j.compstruct.2013.07.028.

[28] A. I. Selmy, N. A. Azab, and M. A. Abd El-Baky, “Flexural fatigue characteristics of two different types of glass fiber/epoxy polymeric composite laminates with statistical analysis,” *Composites Part B: Engineering*, vol. 45, no. 1, pp. 518–527, Feb. 2013, doi: 10.1016/j.compositesb.2012.08.017.

[29] S. Seifoori, R. Izadi, G. H. Liaghat, and A. Mahdian, “An experimental study on damage intensity in composite plates subjected to low-velocity impacts,” *Polymer Testing*, vol. 93, no. September 2020, p. 106887, 2021, doi: 10.1016/j.polymertesting.2020.106887.

[30] W. P. Winfree, J. N. Zalameda, and P. A. Howell, “Improved flaw detection and characterization with difference thermography,” in *Thermosense: Thermal Infrared Applications XXXIII*, May 2011, vol. 8013, p. 80130U. doi: 10.1117/12.883472.

[31] De Giorgi, Marta, Riccardo Nobile, and Fania Palano. "kf Evaluation in GFRP Composites by Thermography." Applied Sciences 11, no. 11 (2021): 5200. doi.org/10.3390/app11115200

[32] Maierhofer, Christiane, Rainer Krankenhagen, Mathias Röllig, Thomas Heckel, Daniel Brackrock, and Mate Gaal. "Quantification of impact damages in CFRP and GFRP structures with thermography and ultrasonics." *In Proceedings of QIRT 2018*, pp. 933-940. DGZfP e. V., 2018.

[33] C. Colombo and L. Vergani, "Influence of delamination on fatigue properties of a fibreglass composite," *Composite Structures*, vol. 107, pp. 325–333, 2014, doi: 10.1016/j.compstruct.2013.07.028.

[34] Colombo, Chiara, Flavia Libonati, F. Pezzani, Antonio Salerno, and L. Vergani. "Fatigue behaviour of a GFRP laminate by thermographic measurements." *Procedia Engineering* 10 (2011): 3518-3527.

[35] W. Harizi, S. Chaki, G. Bourse, and M. Ourak, "Mechanical damage assessment of Polymer-Matrix Composites using active infrared thermography," *Composites Part B: Engineering*, vol. 66, pp. 204–209, 2014, doi: 10.1016/j.compositesb.2014.05.017.

[36] S. G. Zacharia, A. O. Siddiqui, and J. Lahiri, "NDT & E International In situ thermal diffusivity determination of anisotropic composite structures : Transverse diffusivity measurement," *NDT and E International*, vol. 48, pp. 1–9, 2012, doi: 10.1016/j.ndteint.2012.01.009.

[37] R. Steinberger, T. I. Valadas Leitão, E. Ladstätter, G. Pinter, W. Billinger, and R. W. Lang, "Infrared thermographic techniques for non-destructive damage characterization of carbon fibre reinforced polymers during tensile fatigue testing," *International Journal of Fatigue*, vol. 28, no. 10, pp. 1340–1347, 2006, doi: 10.1016/j.ijfatigue.2006.02.036.

[38] Winfree, William P., Joseph N. Zalameda, and Patricia A. Howell. "Improved flaw detection and characterization with difference thermography." In Thermosense: Thermal Infrared Applications XXXIII, vol. 8013, p. 80130U. *International Society for Optics and Photonics*, 2011. doi.org/10.1117/12.883472

[39] Pietrak, Karol, and Tomasz S. Wisniewski. "A review of models for effective thermal conductivity of composite materials." *Journal of Power Technologies* 95, no. 1 (2015): 14.

[40] Terentyeva, Valeria, Indika U. Perera, and Nadarajah Narendran. "Analyzing theoretical models for predicting thermal conductivity of composite materials for LED heat sink applications." In IES Annual Conference Proceedings. 2017.

[41] R. Salgado-Delgado *et al.*, "An Analysis of the Thermal Conductivity of Composite Materials (CPC-30R/Charcoal from Sugarcane Bagasse) Using the Hot Insulated Plate Technique," *Advances in Materials Science and Engineering*, vol. 2016, 2016, doi: 10.1155/2016/4950576.

[42] Oskouei, Amir Refahi, and Jalal Yousefi. "Characterization of residual strength in transversely loaded glass-polyester composites by acoustic emission and sentry function." *Materials Today: Proceedings* 5, no. 1 (2018): 381-387. Doi: 10.1016/j.matpr.2017.11.095